

Chandra X-ray observations of Young Clusters II. Orion Flanking Fields Data.

Solange V. Ramírez ¹, Luisa Rebull ¹, John Stauffer ¹, Stephen Strom ², Lynne Hillenbrand ³, Thomas Hearty ⁴, Eugene L. Kopan ⁵, Steven Pravdo ⁴, Russell Makidon ⁶, & Burton Jones ⁷.

ABSTRACT

We present results of Chandra observations of two flanking fields (FF) in Orion, outside the Orion Nebula Cluster (ONC). The observations were taken with the ACIS-I camera with an exposure time of about 48 ks each field. We present a catalog of 417 sources, which includes X-ray luminosity, optical and infrared photometry and X-ray variability information. We have found 91 variable sources, 33 of which have a flare-like light curve, and 11 of which have a pattern of a steady increase or decrease over a 10 hour period. The optical and infrared photometry for the stars identified as X-ray sources are consistent with most of these objects being pre-main sequence stars with ages younger than 10 Myr. We present evidence for an age difference among the X-ray selected samples of NGC 2264, Orion FF, and ONC, with NGC 2264 being the oldest, and ONC being the youngest.

Subject headings: stars: activity — stars: pre-main sequence — X-rays: stars

1. INTRODUCTION

The Orion Nebula is one of the best studied star formation regions in the Galaxy. The Orion Nebula Cluster (ONC) designates the inner 3 pc (~ 20 arcmin) from θ^1 C Orionis, and contains more than three thousand stars. The core of the ONC, also known as the Trapezium Cluster (Trumpler 1931; Herbig & Terndrup 1986), comprises the stars located within 0.3 pc (~ 2 arcmin) of θ^1 C Orionis, it has an inferred stellar density of about 8000 stars pc⁻³ and it is one of the densest

¹Spitzer Science Center, Mail Stop 220-06, California Institute of Technology.

²NOAO, Kitt Peak National Observatory

³Astronomy Department, California Institute of Technology.

⁴Jet Propulsion Laboratory

⁵IPAC, California Institute of Technology.

⁶Space Telescope Science Institute

⁷Astronomy Department, California Institute of Technology.

known region of star formation (McCaughrean & Stauffer 1994). Most of the ONC members are visible, primarily because the massive stars in the Trapezium Cluster have swept the gas from the molecular cloud creating a cavity facing towards us. The structure, dynamics and stellar content of the ONC have been extensively studied (Hillenbrand 1997; Hillenbrand et al. 1998; Hillenbrand & Carpenter 2000; Carpenter 2000; Luhman et al. 2000; O’Dell 2001). The stars in the ONC are less than 1 Myr old and their masses range from $<0.05 M_{\odot}$ to $\sim 50 M_{\odot}$ (Hillenbrand 1997; Hillenbrand & Carpenter 2000). Studies of the outer regions of the Orion Nebula (Flanking Fields) have revealed the presence of young stars of ages between 1 and 3 Myrs old (Rebull et al. 2000; Gullbring et al. 1998; Hartmann 1998), with an accretion disk fraction of about 40% (Rebull et al. 2000). The Orion Nebula provides an excellent laboratory for studying pre-main sequence (PMS) stars, given its proximity (470 pc), its age and its stellar diversity.

PMS stars are strong X-ray emitters; typical PMS stars have X-ray luminosities 10^1 to 10^4 above those observed in older main sequence stars (Feigelson & Montmerle 1999). The X-ray emission in low mass stars comes from magnetic reconnection. In the dynamo model, the strength of the magnetic field, and hence the X-ray activity, depends on the rate of differential rotation and on the depth of the outer convective envelope (Gilman 1983; Rosner et al. 1985). There is a clear relationship between rotation rate (period) and X-ray luminosity (L_x) found in late-type stars in clusters as old as NGC 2547 (15-40 Myrs, Jeffries et al. 2000) through the Hyades (~ 500 Myrs, Stauffer et al. 1997). The ratio between the X-ray and bolometric luminosity, L_x/L_{bol} , increases with increasing rotation rate, until the most rapidly rotating stars reach a maximum X-ray luminosity (or saturation level) such that $L_x/L_{bol} \sim 10^{-3}$ (see Pizzolato et al. 2003, and references within). It is much less clear that rotation and L_x/L_{bol} are related in younger clusters. Gagne & Caillault (1994) studied a 4.5 square degree region centered in the Orion Nebula, using X-ray data from the Einstein Observatory. They found that at least 100 sources were associated with late-type PMS stars, and their X-ray activity was not correlated with published rotational periods and spectroscopic rotational velocities. Gagne et al. (1995) used ROSAT X-ray data in a similar study in the Orion Nebula, finding no dependence of X-ray activity on rotation. More recently, the Chandra Observatory has provided significantly improved spatial resolution and sensitivity for X-ray observations. Feigelson et al. (2002) reported X-ray observations of the ONC using the Chandra Observatory ACIS-I detector. They found more than a thousand X-ray sources, 91% of them associated with known stellar members of the cluster. Feigelson et al. (2003) also see no obvious correlation between rotation and L_x/L_{bol} for their ONC sample, and conclude that the X-ray generation mechanism for young PMS stars must be different from that responsible in young main sequence stars. Flaccomio et al. (2003b) analyzed data for a number of young associations and clusters (including Orion), and agree that there is little correlation between L_x/L_{bol} and rotation at very young ages, but conclude that the data are consistent with a single physical mechanism, where the Orion-age stars are simply all at or near the saturation level. We intend to use our Orion flanking field data and other new Chandra data for NGC 2264 Ramírez et al. (2004) to help determine at what age the relationship between rotation and L_x/L_{bol} emerges.

In the present paper, we present results of Chandra observations of two of the flanking fields (FF) in the Orion Nebula (fields #2 & #4 from Rebull et al. 2000), just outside the ONC. We discuss source detection, variability and L_x determination, providing a catalog of 417 X-ray sources. We present evidence that the X-ray selected sample of PMS stars in the flanking fields in Orion are older than a similarly selected sample in the ONC. In paper III (Rebull et al. 2004), we will discuss in more detail the relationships found here between rotation rate, mass accretion rate, disk indicators, and X-ray luminosity, in our field of NGC 2264 and the two Orion flanking fields.

2. OBSERVATIONS

Two flanking fields in Orion were observed with the Advanced CCD Imaging Spectrometer (ACIS) detector on board the *Chandra X-ray Observatory* (Weisskopf et al. 2002). The imaging array (ACIS-I) consists of four 1024×1024 front-side illuminated CCDs and covers an area on the sky of about 17′×17′. The North Orion Flanking Field (NOFF) is centered at $5^h35^m19^s$, $-4^\circ48'15''$, about 36′ (~ 5 pc, at a distance of 470 pc) north of the Trapezium Cluster, and it was observed on 2002 August 26 with a total exposure time of 48.8 ks. The South Orion Flanking Field (SOFF), centered at $5^h35^m6^s$, $-5^\circ40'48''$, about 17′ (~ 2.5 pc, at a distance of 470 pc) south of the Trapezium Cluster, was observed on 2002 September 6 with a total exposure time of 47.9 ks. Figure 1 shows a $1^\circ \times 1.5^\circ$ image of Orion from the Palomar Digital Sky Survey (Reid et al. 1991), with both Chandra ACIS-I fields of view marked as boxes. The fields were selected to maximize the number of stars in the field of view with known periods from Rebull (2001) and with minimal overlap with other contemporaneous Chandra Orion observation (Feigelson et al. 2002; Flaccomio et al. 2003b).

2.1. Data Preparation

Data analysis was performed in the same manner as described in Ramírez et al. (2004), where we discussed similar observations of a field in NGC2264. In summary, we started with the Level 1 processed event list, applied charge transfer inefficiency (CTI) correction as described in Townsley et al. (2000), then filtered by ASCA grades; by time intervals; and by background flaring due to solar activity. Removal of the background flares identified by the latter step reduced the exposure time to 46.9 ks for the NOFF and to 46.3 ks for the SOFF. Finally, the energy range was restricted to 0.3 – 10 keV. The filtering process was done using the Chandra Interactive Analysis of Observations (CIAO) package¹. Figures 2 and 3 show the ACIS-I image of the filtered observations for the NOFF and the SOFF, respectively.

¹<http://cxc.harvard.edu/ciao/index.html>

2.2. Source detection

X-ray sources were identified using the *wavdetect* tool within the CIAO package. The *wavdetect* tool works well in detecting X-ray sources in crowded fields. This tool performs a Mexican hat wavelet decomposition and reconstruction of the image as described in Freeman et al. (2002). We used wavelet scales ranging from 1 to 16 pixels in steps of $\sqrt{2}$, and the default source significance threshold of 1×10^{-6} . The *wavdetect* tool was run separately in the four ACIS-I CCDs images for both fields and it produced an original list of 256 sources for the NOFF and 280 sources for the SOFF (see Sec 3.1).

2.3. Astrometric Alignment

The positions of the sources obtained by *wavdetect* were correlated with 2MASS positions. Each X-ray source was manually checked to confirm that the 2MASS counterpart lay within the radius for count extraction (as defined in Ramírez et al. (2004)). We checked the astrometry of the Chandra observations using all X-ray sources located within an off-axis angle (ϕ) less than 5 arcmin that have 2MASS counterparts. A total of 85 NOFF sources and 70 SOFF sources meet this criteria. We determined a mean offset in R.A. of $-0.09'' \pm 0.02$ and a mean offset in DEC of $-0.14'' \pm 0.03$ between the NOFF Chandra and 2MASS coordinates and a mean offset in R.A. of $0.09'' \pm 0.03$ and a mean offset in DEC of $-0.28'' \pm 0.03$ between the SOFF Chandra and 2MASS coordinates. The Chandra positions were corrected by these mean offsets to put the X-ray sources in the same reference frame as their 2MASS counterparts.

3. RESULTS

3.1. X-ray Photometry

X-Ray aperture photometry was initially performed on the 536 sources detected by the CIAO tool *wavdetect*. The radius for count extraction, R_{ext} , and the annulus for background determination were defined in the same manner as in Ramírez et al. (2004). The X-ray counts (C_{extr}) and background counts were extracted using the CIAO tool *dmextract*. We computed the background in counts \times arcsec $^{-2}$ as a function of off-axis angle (ϕ), performing a 3σ rejection fit to avoid background counts from annuli that have other sources within. The computed background was constant as a function of ϕ , and it had a value of $B=(0.072\pm 0.024)$ counts \times arcsec $^{-2}$ for the NOFF and a value of $B=(0.059\pm 0.021)$ counts \times arcsec $^{-2}$ for the SOFF. The net count, $N. C.$ and the count rate, $C. R.$ were computed for each source as in Ramírez et al. (2004).

We carefully inspected the light curves of all the sources (see Sec. 3.3) and their appearance in the image of the Chandra field of view. A total of 119 (22%) sources were rejected from the original list: 107 sources had light curves consistent with cosmic ray afterglows, 5 sources were detected

twice, since *wavdetect* was run separately in each CCD, and 7 sources were located at the edge of the field of view. Of the 107 light curves having a cosmic ray shape, 106 (99%) contain cosmic ray afterglows flagged by the pipeline. Our final list of 417 X-ray sources (203 from the NOFF, 214 from the SOFF) is provided in Table 1.

3.2. X-ray Luminosities

We selected all sources with more than 500 net counts, extracted their spectra and fit them to measure their X-ray fluxes. A total of 24 sources from the NOFF and 20 sources from the SOFF meet this criteria and they are listed in Table 2. The spectra were extracted within R_{ext} using the CIAO tool *dmextract*. The spectra of the NOFF and the SOFF sources are shown in Figures 4 and 5, respectively. We used the same spectral fitting process, as described by Ramírez et al. (2004), with the Redistribution Matrix Files (RMF) provided by the CTI corrector (Townsend et al. 2000), Auxiliary Response Files (ARF) created by the CIAO tool *mkarf* and later corrected for the ACIS low energy quantum efficiency degradation. We adopted a photoelectric absorption model (*xswabs*), which uses Wisconsin cross sections from Morrison & McCammon (1983). This model has one parameter that is the equivalent hydrogen column density (nH). The hydrogen column density was fixed to a value of $0.08 \times 10^{22} \text{ cm}^{-2}$ to match an extinction value of $A_V = 0.41$, which is the most likely value of the observed extinction towards both Orion flanking fields (see Rebull et al. 2000, for more discussion). As discussed in Ramírez et al. (2004), the error in L_x that comes from fixing nH is negligible. Finally, we adopted a thermal emission model (*xsmekal*) based on the model calculations of Mewe et al. (1985, 1986), and Kaastra (1992) with Fe L calculations by Liedahl et al. (1995). This model includes line emissions from several elements. The remaining two parameters in the model are the plasma temperature (kT) and a normalization factor. As in the analysis of NGC 2264 Chandra observations (Ramírez et al. 2004), we used a two temperature model to fit the X-ray spectra. The spectral parameters obtained from the two plasma temperature models are listed in Table 2. The X-ray flux for the brightest sources is determined from the best spectral model derived from the mean model parameters. We computed mean plasma temperatures of (0.63 ± 0.05) keV and (2.6 ± 0.3) keV for the NOFF sources and mean plasma temperatures of (0.77 ± 0.05) keV and (2.9 ± 0.2) keV for the SOFF sources. The mean plasma temperatures are held constant and the integration of the best fit between 0.3 and 8.0 keV provides the X-ray flux. The resulting X-ray fluxes are listed in Table 2.

We use the X-ray fluxes of the bright sources to compute a X-ray flux weighted conversion factor between count rate and X-ray flux. We obtained a conversion factor of $(6.58 \pm 0.13) \times 10^{-15}$ ($\text{erg/cm}^2/\text{s})/(\text{counts/ks})$ for the NOFF sources and a conversion factor of $(6.72 \pm 0.20) \times 10^{-15}$ ($\text{erg/cm}^2/\text{s})/(\text{counts/ks})$ for the SOFF sources. The values of these conversion factors are in reasonably good agreement with the derived conversion factor for our similar X-ray observation in NGC 2264 ($6.16 \pm 0.13 \times 10^{-15}$ ($\text{erg/cm}^2/\text{s})/(\text{counts/ks})$) Ramírez et al. 2004) and other published values (see Ramírez et al. 2004). The X-ray flux for our catalog of X-ray sources in both Orion

fields is listed in column 10 of Table 1. The X-ray luminosity, L_x , listed in column 11 of Table 1, is computed assuming a distance to Orion of 470 pc.

The limiting luminosity in our X-ray observations varies within the field of view, because of the variation of the PSF across the field. The faintest source is located at $\phi \sim 6'$ and it has a count rate of 0.08 counts/ks, corresponding to a X-ray luminosity of 28.15 at the distance of Orion. About 85 % of our sources are located within $\phi = 8'$. At that off-axis angle the limiting count rate has increased to 0.20 counts/ks, corresponding to a X-ray luminosity of $\log(L_x)=28.5$ at the distance of Orion. At $\phi = 10'$, we cannot detect X-ray sources fainter than 0.45 counts/ks ($\log(L_x) = 28.9$). Therefore, we adopt a value of $\log(L_x)=28.5$ dex as the limiting X-ray luminosity for our observations, keeping in mind that this value holds for sources located within $\phi \sim 8'$.

3.3. Variability

Light curves were determined for all 417 sources detected by *wavdetect* using the CIAO tool *lightcurves* with a bin time of 2500 s. The statistics of the light curves of the sources of our X-ray catalog were obtained using the Xronos ² tool *lcstats*. This provides, among other values, the probability of the light curve being constant, $P_c(\chi^2)$, as derived from the Chi-square value. The $P_c(\chi^2)$ values are listed in column 12 of Table 1. The light curves of the sources with $P_c(\chi^2) < 90\%$ were analyzed further, since they are the most likely to be variable. We defined a variable source as those having 2500 s bin light curves with $P_c(\chi^2) < 90\%$, and 5000 s and 7500 s bin light curves with reduced $\chi^2 > 2.5$, as in Ramírez et al. (2004). There are 91 variable sources that meet this criteria. Variable sources are marked with a 'v' in column 13 of Table 1. There are 33 variable sources which show a flare shape, defined as a rapid increase and a slow decrease in the X-ray flux. Variable sources with a flare-like light curve are marked with an additional 'f' in column 13 of Table 1. There are sixteen sources that show a possible flare pattern, described as an increase in X-ray flux happening at the end of our observations or a decrease in X-ray flux occurring at the beginning of our observations. Variable sources with a possible flare pattern are marked with an additional 'p' in column 13 of Table 1. We have detected a fraction of about 11% flaring sources (8% excluding possible flares) in both Orion flanking fields. A comparable fraction (about 8%) was observed in a similar length observation in NGC 2264 (Ramírez et al. 2004). There are 11 sources that show a steady increase or decrease in their X-ray flux. Those sources are marked with an additional 's' in column 13 of Table 1. A similar pattern is observed in two NGC 2264 sources (Ramírez et al. 2004) and three X-ray IC 348 sources (Preibisch & Zinnecker 2002). These patterns might be understood by rotational modulation of X-ray flares (Stelzer et al. 1999). In Figure 6, we show a selection of light curves of sources of comparable luminosity. In the top panels, we show two light curves with a flare shape; in the middle-top panels, there are two sources that show a steady decrease in their X-ray flux; in the middle-bottom panels, there are two variable light curves. Finally in the bottom

²<http://heasarc.gsfc.nasa.gov/docs/xanadu/xronos/xronos.html>

panels, two constant light curves are plotted.

4. DISCUSSION

4.1. Description of the optical/infrared catalog

We correlated the X-ray sources with a catalog of optical and near-IR stars in the Orion region; see Tables 3 and 4. We constructed the catalog by merging ~ 30 published catalogs of optical and infrared photometry, spectral types, previous X-ray detections, proper motion surveys, periods, and spectroscopic projected rotational velocities ($v \sin i$). Although our X-ray data presented are located in two flanking fields (#2 and #4 from Rebull et al. 2000), we constructed a catalog over this whole region in an attempt to increase the number of stars with known L_x and optical counterparts.

The optical photometry were taken from Rebull et al. (2000), Hillenbrand (1997), Stassun et al. (1999), Wolff et al. (2003), and Gagne et al. (1995), in that order. For near-IR photometry, Carpenter et al. (2001) averaged over their light curves, presenting the most reliable average JHK magnitude. Magnitudes for the remaining stars then came from 2MASS, Muench et al. (2002), Hillenbrand et al. (1998), and Hillenbrand & Carpenter (2000), in that order. Spectral types were taken in this order: Rebull et al. (2000), Hillenbrand (1997), Herbig & Bell (1988), Duncan (1993), Edwards et al. (1993), Smith et al. (1983), Walker (1969, 1983), Gagne & Caillault (1994), Gagne et al. (1995), and Wolff et al. (2003). Gagne & Caillault (1994) and Gagne et al. (1995) collected much of the optical and spectroscopic literature for stars in this region, reporting on X-ray detections using Einstein and ROSAT, respectively. Strom et al. (1990) analyzed Einstein data for some stars in this region. The largest X-ray data base, and the one obviously most similar to our own data, is Feigelson et al. (2002); these Chandra ACIS X-ray detections are in the ONC region; their fields have marginal spatial overlap with the observations reported here. Finally, there are several surveys in this region devoted specifically to obtaining rotation data. Periods were taken from Rebull (2001), Stassun et al. (1999), Herbst et al. (2000, 2001), Carpenter et al. (2001), Gagne et al. (1995), in that order. Spectroscopic rotational velocities came from Rhode et al. (2001), Wolff et al. (2003), Duncan (1993), Smith et al. (1983), Gagne et al. (1995), Hartmann et al. (1986), and finally Walker (1980).

4.2. Comparison of optical/infrared and X-ray Catalogs

We found that 356 (85%) of our 417 X-ray sources have optical and/or infrared counterparts (130 (31%) have known periods). Each X-ray source was manually checked to confirm that the optical and/or infrared counterparts lay within the radius for count extraction (R_{ext} , as defined in Ramírez et al. (2004)). The 356 sources and their corresponding optical and/or infrared photometry

are listed in Table 3. Other names of the sources given by the different catalogs used in our compilation are listed in Table 4.

There were cases in which two optical/near-IR counterparts were located within R_{ext} , which is a measure of the size of the PSF in the Chandra field. This was the case for 9 X-ray sources, shown in Figure 7. These sources are marked with a 'c' in Table 1 and are matched to the closest counterpart in each case. Source N134 seems to have two components separated by $\sim 1''$. The optical (Par 1970) and 2MASS counterparts coincide with the weaker component. Par 1970 is a B2 star, which should be weak in X-rays. Source N217 has two pairs of optical and 2MASS counterparts separated by $\sim 6.5''$. Source S025 has two pairs of optical/2MASS counterparts within the extraction circle. One pair is at the edge of the extraction circle and the other within $1.3''$ of the X-ray position. Source S091 is an extended source, possibly with two components. Source S101 has two optical and one infrared source within the extraction circle. Source S141 has two optical sources within the extraction circle. Source S182 has a large aperture and its extraction circle contains emission from a nearby X-ray source. Sources S187 and S191 are separated by $5.5''$ at an off axis angle of about $8.5'$. Their circles of extraction ($R_{ext} \sim 10''$) overlap considerably. Source S187 has an optical counterpart (Par 1897), while source S191 has an infrared counterpart (2MASS J05351696-0532464). Optical and/or infrared spectroscopy of these objects may help determine the true counterpart of these X-ray sources.

There are 902 stars in our optical/infrared catalog with J , H , and K photometry and with positions inside the field of view of our Chandra observations. Among those 902 stars, 316 (35%) have X-ray Chandra counterparts. Figure 8 shows a J magnitude histogram of all the 902 stars with J , H , and K photometry and positions inside the Chandra field (solid line) and the histogram of the 316 X-ray Chandra counterparts (dotted line). The completeness limit of the infrared sample is that of 2MASS. We can see in Figure 8 that our infrared sample goes deeper than the sample of stars with X-ray counterparts. A similar behavior is seen in the optical sample histogram. This means that all the X-ray sources should have been matched to sources in our optical/infrared catalog if they are associated with stars earlier than M4 at the distance of Orion in the absence of extinction.

Among the Orion X-ray sources in our catalog, 130 (31% of the 417 X-ray source) have known periods from Rebull (2001). Among the Orion X-ray sources with known periods, 46 (35% of the 130 X-ray sources with known periods) are classified as variable X-ray sources, and 24 (18% of the 130 X-ray sources with known periods) show a flare or possible flare pattern. Nearly 52% of the 46 flaring X-ray sources are periodic in optical wavelengths, while only 31 % of all the X-ray sources show a periodic optical variation. There are twelve sources with short enough optical periods so that a significant fraction of the period is observed in the time length of the X-ray Chandra observations. However, the low signal to noise of the light curves and the presence of X-ray flares prevent us from drawing any conclusions regarding the presence or absence of rotational modulation of the X-ray flux.

There are 61 X-ray sources that do not have optical or infrared counterparts and they are marked with a 'x' in column 13 of Table 1. Based on the limiting magnitude of our optical catalog ($V \sim 20$ mag), the X-ray to optical flux ratio, f_X/f_V , of the sources with only X-ray detection is $\gtrsim 10^{-2.3}$. Therefore, these sources could be either late M dwarfs or extragalactic objects (Stocke et al. 1991). Given the presence of a dark cloud behind Orion, the detection of background M dwarfs in X-rays is unlikely, so, if these sources detected only in X-rays are M dwarfs, then they should be $r \leq 470$ pc. We have identified 17 of these sources detected only in X-rays with sources in a deep 2MASS image (Kopan 2004, priv comm, ~ 2 magnitudes deeper than the 2MASS All Sky Point Source Catalog) reducing the number of sources detected only in X-rays to 44. Based on the limiting flux of our X-ray sample, the maximum X-ray luminosity of M dwarfs (Fleming et al. 1995), and the limiting magnitude of the deep 2MASS image, we determined that all foreground M dwarfs present in our X-ray sample should have been detected in the deep 2MASS image. Source counts in the Chandra South and North Deep Fields (Rosati et al. 2002; Brandt et al. 2001) predict the presence of about 20 AGN in each ACIS field of view at the flux limit of our observations and assuming a Galactic extinction of $A_V \sim 11$ magnitudes (from NED extinction calculator³). Feigelson et al. (2002) found 101 X-ray sources with no optical counterparts in their 82 ks Chandra observation of the ONC, all highly concentrated towards the center of the ONC. They argued that most of those sources were indeed heavily embedded protostars or young stars seen behind the cloud. They estimated that the extragalactic contamination cannot be more than 15 objects, due to the high extinction of the ONC behind the stars. In our case, the extinction in front of the Orion flanking field stars is significantly lower than on the ONC (Rebull et al. 2000) and our only X-ray sources seem to be concentrated in areas of low extinction determined from a CO map of the area (Bally et al. 1987) and $H - K$ color of 2MASS sources in those areas. Thus, we believe that the most likely explanation is that most of the objects detected only in X-rays are active galaxies. Deeper infrared photometry or deeper X-ray observations may help determine the true nature of these sources.

There are 17 stars for which rotation and spectral type information exist in our optical/infrared catalog, and for which no X-ray counterpart was found. In order to allow us to use these stars in the next paper, we determined upper limits for their X-ray luminosity in the same manner as Ramírez et al. (2004). The upper limit for the X-ray luminosity was computed assuming a distance to Orion of 470 pc. The upper limit results are listed in Table 5.

4.3. Color-Color diagram.

In Figure 9, we have plotted the $J - H$, $H - K$ color-color diagram of all the infrared sources in the field of view of our Chandra observation. Most of the X-ray sources with infrared colors are located near the locus of the classical T-Tauri (CTT) stars (Meyer et al. 1997). The remaining

³<http://nedwww.ipac.caltech.edu/forms/calculator.html>

sources are located within the reddening vectors of late main sequence stars and CTT stars.

4.4. Color-Magnitude Diagrams.

There are 445 stars in our optical/infrared catalog with I_c and V photometry and with positions inside both fields of view of the Chandra observations. Among those 445 stars, 280 (63 %) have X-ray Chandra counterparts. In Figure 10, we have plotted $(V - I_c) - M_{I_c}$ color magnitude diagrams of the optical sources in the fields of view of our Chandra observations. The dereddened $V - I_c$ color and the absolute magnitude M_{I_c} were obtained assuming an average extinction of $A_V = 0.41$ (Rebull et al. 2000), and dereddening relationships from Fitzpatrick (1999) and Mathis (1990). In both panels, we have also plotted isochrones from D’Antona & Mazzitelli (1998), as a reference. The dashed line corresponds to $M_{I_c} = 8.75$ mag., which is the lower limit for a low mass Orion member rotating at the saturation level ($\log(L_x/L_{bol}) = -3$) with $\log(L_x) = 28.5$ (limit luminosity of our X-ray sample). This means that the most slowly rotating stars earlier than M3 with optical counterparts should be detected by our X-ray sample.

Most of our X-ray sources are younger than 10^7 years at the distance of Orion, and furthermore the X-ray sources are heavily concentrated between the 10^5 and the 3×10^6 year old isochrones with respect to the general population. Stars that are strong X-ray emitters are likely to be young stars and therefore true members of the Orion cluster. In Rebull et al. (2000), as a result of the lack of membership information for stars this far from the Trapezium, a provisional membership criterion was defined. A line was drawn through an empirically-discovered gap nearly coincident with the 3 Myr isochrone to divide the stars clumping above it in a locus (likely members) from the ones below it (likely field stars). This approximation was supported in Rebull (2001) by the locations of the periodic stars, also likely young and therefore members. The clustering of the X-ray sources above the 3 Myr isochrone is additional confirmation that stars in the locus are more likely to be true members of the cluster than stars below this locus.

There is one star (S038) with M_{I_c} brighter than 0 magnitude. Its optical counterpart, Par 1605, has a spectral type of A0V. It has $\log(L_x) = 30.1$ and $L_x/L_{bol} = 10^{-5.7}$. X-ray emission from late B stars and early A stars is rare, since they are in the transition between wind driven X-ray emission from hot stars and magnetically driven coronae from late type stars. It is often speculated that the X-ray emission observed in late B and early A stars comes from unseen late type companions (Stelzer et al. 2003; Daniel et al. 2002), that explanation could apply to Par 1605.

There are 3 X-ray sources that appear to be much older than 10^7 years. One of them (141S), has unreliable photometry because of background contamination from a nearby star. The other sources (N068 and S115) lack both spectral type and membership information. If we deredden sources N068 and S115 (see Figure 9) along reddening vector towards the locus of CTT stars, we derive a A_V value of 5.9 magnitudes for source N068 and A_V value of 2.1 magnitudes for source S115. The locations of sources N068 and S115 are indicated along with their dereddened positions

in Figure 9. In Figure 11, we have plotted the $(J - H) - M_J$ color magnitude diagram of all the infrared sources with X-ray counterparts, with isochrones from D’Antona & Mazzitelli (1998). The locations of sources N068 and S115 are indicated along with their possible dereddened position. It is possible that these two objects are the youngest and most embedded of our X-ray sources, if they are indeed members of the Orion complex. The unusual optical colors of these sources could be explained by scattered light from an edge on disk.

4.5. Age Difference.

Figure 12 shows the dereddened color magnitude diagram for three X-ray selected samples. On the left panel, we plot the NGC 2264 sample from Ramírez et al. (2004), which includes 201 stars showing X-ray emission. The central panel shows Orion FF data from the present work. Finally, the right panel shows 584 X-ray ONC sources (Feigelson et al. 2002) that have optical counterparts from our database. The stars from the three samples have been dereddened using the following criteria. If the star has a known spectral type, we have used A_I derived from the spectra. For the remaining stars, we have derived A_I from JHK photometry, assuming that the stars are PMS stars. We use A_I from infrared colors if this is greater than one magnitude. If not, we use the median A_I for each field ($A_I=0.25$ for NGC 2264, $A_I=0.25$ for Orion FF, and $A_I=1.31$ for the ONC, Herbig & Terndrup 1986). This criterion is reasonable for fields with variable reddening, as the ONC, where A_I can be as high as 4 magnitudes.

There are several notable differences among the shown CMDs. NGC 2264 stars appear to be more compactly distributed than the ONC stars. There are fewer high mass stars in the Orion FF sample than in the ONC sample. The NGC 2264 sample appears to be the oldest of the three samples. One way to quantify these differences is through the use of statistical boxes. We have divided each X-ray selected sample into smaller samples containing stars of a determined color range of 0.5 magnitudes of width. For each color range we have determined a box, as defined by Tukey (1977) (see also Cleveland 1993). The central horizontal line in each box is the median M_{I_c} for the range in $(V - I_c)_o$ color, while the bottom and the top of the box shows its inter-quartile range (containing 50% of the sample), and the vertical lines coming out of the box mark the position of the adjacent points of the sample (most extreme values in the sample that are not more than 1.5 times the inter-quartile range). In Figure 13 we show the box plots for the three samples together with isochrones from D’Antona & Mazzitelli (1998). We have only plotted the boxes that overlap with all three samples, are within the range of isochrones ($(V - I_c)_o > 1.0$), and are not subject to biases from the optical limit of the catalog or other intrinsic properties ($(V - I_c)_o < 2.5$; Rebull 2001). We have also plotted in the three panels horizontal dotted lines that correspond to the median value of the Orion FF boxes. The median, upper and lower quartile M_{I_c} values are listed in Table 6 for each of the $(V - I_c)_o$ color ranges and for three the samples of X-ray sources. All the NGC 2264 medians are systematically lower than the Orion FF medians, with a mean difference of 0.3 magnitudes ($\sigma=0.1$). All the ONC medians are systematically higher than the Orion FF

medians, with a mean difference of 0.3 magnitudes ($\sigma=0.1$). The effect of reddening is very small, since the reddening vectors go almost parallel to the isochrones. If we used the median reddening for each field, we find the same mean differences in the median M_{I_c} for each color range. If we used a A_V one magnitude higher or one magnitude lower, we get again the same differences in the median M_{I_c} .

The observed differences can be explained by a difference in age among the three samples. Using the D’Antona & Mazzitelli (1998) isochrones, we derive an age of ~ 2 Myrs, ~ 1 Myrs, and ~ 0.5 Myrs for the X-ray selected samples of NGC 2264, Orion FF, and ONC, respectively. Alternatively, assuming vertical Hayashi tracks, stellar luminosities scale as $L \sim t^{-2/3}$ (Hartmann 1998). Thus, differences in luminosity of 0.3 magnitudes corresponds to ratios in age of a factor of ~ 1.5 . Searching for young stars in X-rays is known to be a efficient way of finding young stars (for example, the RASS, e.g., Neuhaeuser et al. 1995). Does the age difference for the **X-ray selected** stars in the three regions apply as well for all low mass members in the three regions? Our own belief is that X-ray selection does not bias YSO population statistics in terms of age and mass (e.g. Feigelson et al. 2002) and therefore our age estimates should be valid for the entire set of stars in the three regions. We caution however that X-ray selection may result in bias for other physical parameters, such as rotation or disk properties (e.g. Flaccomio et al. 2003a,b). In order to provide some support to our assertion concerning X-ray selection bias and age, we have constructed plots like Figure 13 for low mass members of the three clusters located within the Chandra field of view but not restricted to X-ray detection. We derived box-plots for the optical sample of likely members in all three regions using two different reddening prescriptions - one with a mean reddening for each field, and one where we derived reddening exactly as for Figure 13. In both cases, we derived similar ages and age differences for the three fields. We note that this result differs from that reported in Rebull et al. (2000) and Rebull (2001), where no age difference was found between optical samples in the ONC and the Orion flanking fields. The earlier studies used larger fields and a different statistical method that may have smeared out any age differences that might be present. We note that none of the essential conclusions in earlier papers change in any way if the Orion flanking fields are indeed older (or contain a range of older ages) than the ONC.

5. CONCLUSIONS

We present a catalog of Orion X-ray sources from two flanking fields. The observations were taken with the ACIS-I on board the Chandra X-ray Observatory. The catalog, consisting of 417 sources, includes X-ray luminosity, optical and infrared photometry and X-ray variability information. We found 91 variable sources, 33 of which have a flare like light curve, and 11 of which have a pattern of a steady increase or decrease. From the optical and infrared counterparts of the X-ray sources, we have learned that most of the X-ray sources have colors consistent with CTTs that are younger than 10^7 years. We argue that the data are consistent with an age difference among the X-ray selected samples of NGC 2264, Orion FF, and ONC, with NGC 2264 being the oldest, and

ONC being the youngest.

This catalog of X-ray sources will be used to study the relationship between rotational properties and X-ray characteristics of Orion and NGC 2264 stars in paper III (Rebull et al. 2004). We plan to discuss correlations of L_x/L_{bol} with rotation rate (period and $v\sin i$), disk indicators ($I_c - K$, $H - K$, $U - V$, and $H\alpha$), and mass accretion rate as derived from $U - V$ excess. We will also compare the L_x/L_{bol} values found here with those from other young clusters.

We thank the anonymous referee for her/his careful review of the manuscript. Financial support for this work was provided by NASA grant GO2-3011X. This research has made extensive use of NASA’s Astrophysics Data System Abstract Service, the SIMBAD database, operated at CDS, Strasbourg, France, and the NASA/IPAC Infrared Science Archive, which is operated by the Jet Propulsion Laboratory, California Institute of Technology, under contract with the National Aeronautics and Space Administration. The research described in this paper was partially carried out at the Jet Propulsion Laboratory, California Institute of Technology, under a contract with the National Aeronautics and Space Administration.

REFERENCES

- Bally, J., Stark, A. A., Wilson, R. W., & Langer, W. D., 1987, ApJ, 312, 45L
- Brandt, W. N., Alexander, D. M., Hornschemeier, A. E., Garmire, G. P., Schneider, D. P., Barger, A. J., Bauer, F. E., Broos, P. S., Cowie, L. L., Townsley, L. K., Burrows, D. N., Chartas, G., Feigelson, E. D., Griffiths, R. E., Nousek, J. A., & Sargent, W. L. W., 2001, AJ, 122, 2810
- Carpenter, J., 2000, AJ, 120, 3139
- Carpenter, J., Hillenbrand, L. A., & Skrutskie, M. F., 2001, AJ, 121, 3160
- Cleveland, W.S., 1993, *Visualizing Data*, Hobart Press, Summit, New Jersey
- D’Antona, F. & Mazzitelli, I., 1998, in “Brown Dwarfs and Extrasolar Planets”, ASP Conference Series, eds. R. Rebolo, E. Martin, M.R. Zapatero Osorio, p. 442
- Daniel, K. J., Linsky, J. L., & Gagné, M. 2002, ApJ, 578, 486
- Duncan, D. K., 1993, ApJ, 406, 172
- Edwards, S., Strom, S. E., Hartigan, P., Strom, K. M., Hillenbrand, L. A., Herbst, W., Attridge, J., Merrill, K. M., Probst, R., & Gatley, I., 1993, AJ, 106, 372
- Feigelson, E. D., & Montmerle, T., 1999, ARA&A, 37, 363
- Feigelson, E. D., Bross, P., Gaffney, J. A., Garmire, G., Hillenbrand, L. A., Pravdo, S. H., Townsley, L., & Tsuboi, Y., 2002, ApJ, 574, 258
- Feigelson, E. D., Gaffney, J. A., Garmire, G., Hillenbrand, L. A., & Townsley, L., 2003, ApJ, 584, 911
- Fitzpatrick, E. L., 1999, PASP, 111, 63
- Flaccomio, E., Micela, G., & Sciortino, S., 2003a, A&A, 397, 611
- Flaccomio, E., Micela, G., & Sciortino, S., 2003b, A&A, 402, 277
- Fleming T. A., Schmitt, J. H. M. M., & Giampapa, M. S., 1995, ApJ, 450, 401
- Freeman, P. E., Kashyap, V., Rosner, R., & Lamb, D. Q., 2002, ApJS, 138, 185
- Gagne, M., & Caillault, J.-P., 1994, ApJ, 437, 361
- Gagne, M., Caillault, J.-P., & Stauffer, J. R., 1995, ApJ, 445, 280
- Gilman, P. A., 1983, ApJS, 53, 243

- Gullbring, E., Hartmann, L., Briceño, C. & Calvet, N., 1998, ApJ, 492, 323
- Hartmann, L., 1998, *Accretion Processes in Star Formation* (Cambridge: Cambridge Univ. Press)
- Hartmann, L., Hewett, R., Stahler, S., Mathieu, R. D., 1986, ApJ, 309, 275
- Herbig, G. H., & Terndrup, D. M., 1986, ApJ, 307, 609
- Herbig, G. H., & Bell, K. R., 1988, Lick Observatory Bull. No. 1111, 1
- Herbst, W., Rhode, K. L., Hillenbrand, L. A., & Curran, G., 2000, AJ, 119, 261
- Herbst, W., Bailer-Jones, C. A. L., & Mundt, R., 2001, ApJ, 554, 197L
- Hillenbrand, L., 1997, AJ, 113, 1733
- Hillenbrand, L. A., Strom, S. E., Calvet, N., Merrill, K. M., Gatley, I., Makidon, R. B., Meyer, M. R., & Skrutskie, M. F., 1998, AJ, 116, 1816
- Hillenbrand, L. A., & Carpenter, J., 2000, ApJ, 520, 236
- Jeffries, R. D., Totten, E. J., & James, D. J. 2000, MNRAS, 316, 950
- Jones, B., and Walker, M., 1988, AJ, 95, 1755.
- Kaastra, J. S., 1992, *An X-Ray Spectral Code for Optically Thin Plasmas* (Internal SRON-Leiden Report, updated version 2.0)
- Kraft, R. P., Burrows, D. N., & Nousek, J. A., 1991, ApJ, 374, 344
- Liedahl, D. A., Osterheld, A. L., & Goldstein, W. H., 1995, ApJL, 438, 115
- Luhman, K. L., Reike, G. H., Young, E. T., Cotera, A. S., Chen, H., Reike, M. J., Schneider, G., & Thompson, R. I., 2000, ApJ, 540, 1016
- Mathis, J. S., 1990, ARA&A, 28, 37
- McCaughrean, M. J., & Stauffer, J. R., 1994, AJ, 108, 1382
- Mewe, R., Gronenschild, E. H. B. M., & van den Oord, G. H. J., 1985, A&AS, 62, 197
- Mewe, R., Lemen, J. R., & van den Oord, G. H. J., 1986, A&AS, 65, 511
- Meyer, M. R., Calvet, N., & Hillenbrand, L. A., 1997, AJ, 114, 288
- Morrison, R., McCammon, D., 1983, ApJ, 270, 119
- Muench, A., Lada, E. A., Lada, C. J., & Alves, J., 2002, ApJ, 573, 366

- Neuhaeuser, R., Sterzik, M. F., Schmitt, J. H. M. M., Wichmann, R., & Krautter, J., 1995, *A&A*, 297, 391
- O'Dell, C. R., 2001, *PASP*, 113, 29
- Parenago, P. P. 1954, *Trudy Gos. Astron. Inst. im. Shternberga*, 25, 1
- Park, B.-G., *et al.* 2000, *AJ*, 120, 894
- Pizzolato, N., Maggio, A., Micela, G., Sciortino, S., Ventura, P., 2003, *A&A*, 397, 147
- Preibisch, T. & Zinnecker, H., 2002, *ApJ*, 123, 1613
- Ramírez, S. V., Rebull, L., Stauffer, J., Hearty, T., Hillenbrand, L., Jones, B., Makidon, R., Pravdo, S., Strom, S., & Werner, M., 2004, *AJ*, in press
- Rebull, L. M., Hillenbrand, L. A., Strom, S. E., Duncan, D. K., Patten, B. M., Pavlovsky, C. M., Makidon, R. B., & Adams, M. T., 2000, *AJ*, 119, 3026
- Rebull, L. M., 2001, *AJ*, 121, 1676
- Rebull, L. M., *et al.* in preparation
- Reid, I. N., Brewer, C., Brucato, R. J., McKinley, W. R., Maury, A., Mendenhall, D., Mould, J. R., Mueller, J., Neugebauer, G., Phinney, J., Sargent, W. L. W., Schombert, J., & Thickett, R., 1991, *PASP*, 661
- Rhode, K., Herbst, W., & Mathieu, R. D., 2001, *AJ*, 122, 3258
- Rosati, P., Tozzi, P., Giacconi, R., Gilli, R., Hasinger, G., Kewley, L., Mainieri, V., Nonino, M., Norman, C., Szokoly, G., Wang, J. X., Zirm, A., Bergeron, J., Borgani, S., Gilmozzi, R., Grogin, N., Koekemoer, A., Schreier, E., Zheng, W., 2002, *ApJ*, 566, 667
- Rosner, R., Golub, L., & Vaiana, G. S., 1985, *ARA&A*, 23, 413
- Smith, M. A., Beckers, J. M., & Barden, S. C., 1983, *ApJ*, 271, 237
- Stassun, K., Mathieu, R. D., Mazeh, T., & Vrba, F. J., 1999, *AJ*, 117, 2941
- Stauffer, J. R., Balachandran, S. C., Krishnamurthi, A., Pinsonneault, M., Terndrup, D. M., & Stern, R. A., 1997, *ApJ*, 475, 604
- Stelzer, B., Neuhäuser, R., Casanova, S., & Montmerle, T., 1999, *A&A*, 344, 154
- Stelzer, B., Huéramo, N., Hubrig, S., Zinnecker, H., & Micela, G., 2003, *A&A*, 407, 1067
- Stoeck, J. T., Morris, S. L., Gioia, I. M., Maccacaro, T., Schild, R., Wolter, A., Fleming, T. A., & Henry, J. P., 1991, *ApJS*, 76, 813

- Strom, K. M., Strom, S. E., Wilkin, F. P., Carrasco, L., Cruz-Gonzalez, I., Recillas, E., Serrano, A., Seaman, R. L., Stauffer, J. R., Dai, D., & Sottile, J., 1990, *ApJ*, 362, 168
- Sung, H., Bessell, M., & Lee, S.-W., 1997, *AJ*, 114, 2644
- Tian, K. P., van Leeuwen, F., Zhao, J. L., & Su, C. G., 1996, *A&AS*, 118, 503
- Townsley, L. K., Broos, P. S., Garmire, G. P., & Nousek, J. A., 2000, *ApJ*, 534, 139L
- Trumpler, R. J., 1931, *PASP*, 43, 255
- Tukey, J. W., 1977, *Exploratory Data Analysis*, Addison-Wesley
- Walker, M., 1969, *ApJ*, 155, 447
- Walker, M., 1980, *PASP*, 102, 726
- Walker, M., 1983, *ApJ*, 271, 642
- Weisskopf, M. C., Brinkman, B., Canizares, C., Garmire, G., Murray, S., & van Speybroeck, L. P., 2002, *PASP*, 114, 1
- Wolff, S., Strom, S. E., & Hillenbrand, L. A., 2003, *ApJin* press

Fig. 1.— Image of Orion from the Palomar Digital Sky Survey (Reid et al. 1991). The image has a field of view of $60' \times 90'$ and the boxes represent the fields of view of the Chandra ACIS-I observations. The North Orion Flanking Field (NOFF) is centered at $RA(2000)=5^h 35^m 19^s$, $DEC(2000)=-4^\circ 48' 15''$, and the South Orion Flanking Field (SOFF) is centered at $RA(2000)=5^h 35^m 6^s$, $DEC(2000)=-5^\circ 40' 48''$. (figure available at http://spider.ipac.caltech.edu/staff/solange/ramirez07_figs.ps)

Fig. 2.— Image of the North Orion Flanking Field (NOFF), observed with ACIS-I at the Chandra Observatory. The image has a field of view of $17' \times 17'$ and it is centered at $RA(2000)=5^h 35^m 19^s$, $DEC(2000)=-4^\circ 48' 15''$. This image contains only filtered events. (figure available at http://spider.ipac.caltech.edu/staff/solange/ramirez07_figs.ps)

Fig. 3.— Image of the South Orion Flanking Field (SOFF), observed with ACIS-I at the Chandra Observatory. The image has a field of view of $17' \times 17'$ and it is centered at $RA(2000)=5^h 35^m 6^s$, $DEC(2000)=-5^\circ 40' 48''$. This image contains only filtered events. (figure available at http://spider.ipac.caltech.edu/staff/solange/ramirez07_figs.ps)

Fig. 4.— Spectra of the 24 brightest sources in the NOFF sample. The solid lines show the best two plasma temperature model. (figure available at http://spider.ipac.caltech.edu/staff/solange/ramirez07_figs.ps)

Fig. 5.— Same as Fig.4, but for the 20 brightest sources in the SOFF. (figure available at http://spider.ipac.caltech.edu/staff/solange/ramirez07_figs.ps)

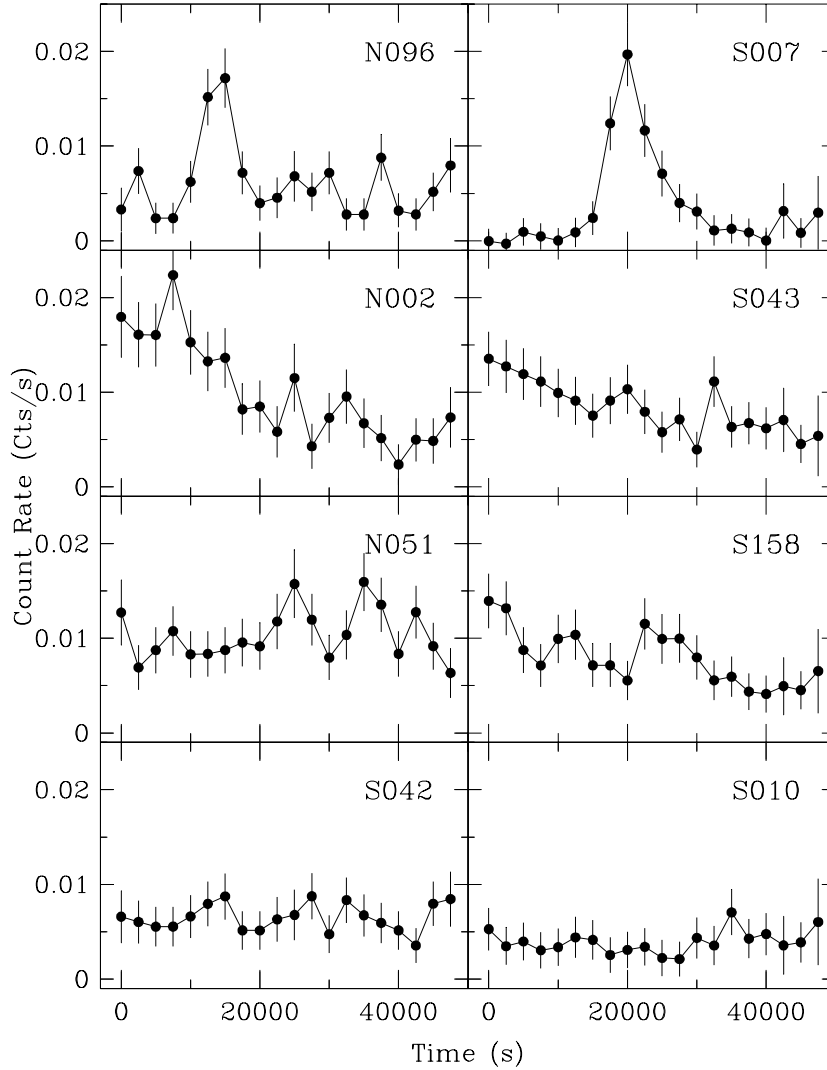


Fig. 6.— Examples of light curves for eight X-ray sources of comparable luminosity from our sample. The two sources in the top panels show flare-like light curves. The two sources on the middle-top panels show a steady decrease in their light curves. The two sources on the middle-low panels are variable, according to our statistical test, and the two sources in the bottom panels are constant. The sources in the left panels are from the NOFF and the sources in the right panels are from the SOFF. There are 91 variable sources in our Orion sample of 417 X-ray objects; 33 of them show a flare-like light curve.

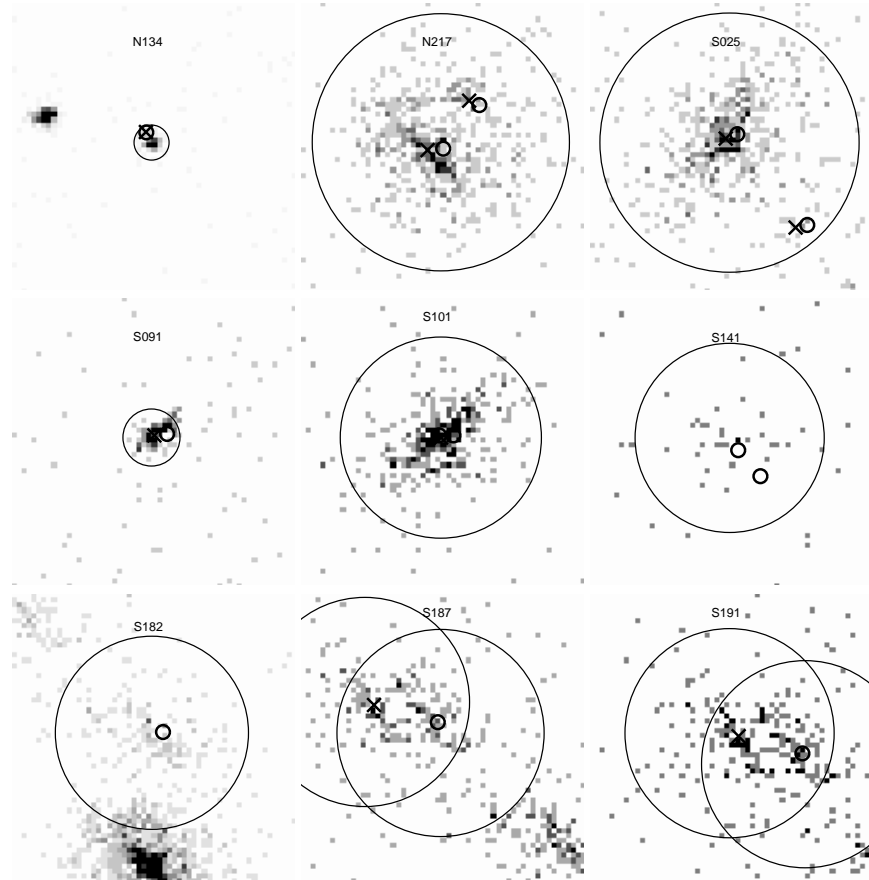


Fig. 7.— Finding charts for 9 sources that show several optical (*circle*) and/or infrared (*cross*) counterparts within their extraction circle (*thin circle*) or have contamination from nearby X-ray sources.

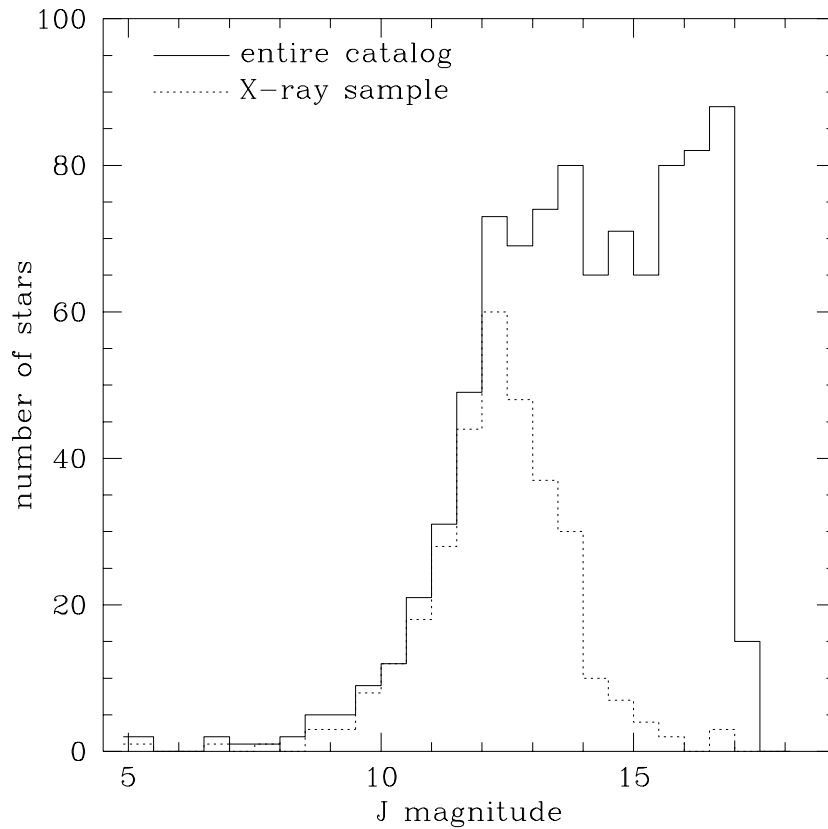


Fig. 8.— J magnitude histogram of all the sources with J , H , and K magnitudes in our Chandra fields. The solid line corresponds to all the sources, and the dotted line corresponds to all the sources with X-ray counterparts. All the X-ray sources should have been matched to sources in our catalog if they are associated with stars earlier than M4 at the distance and age of Orion.

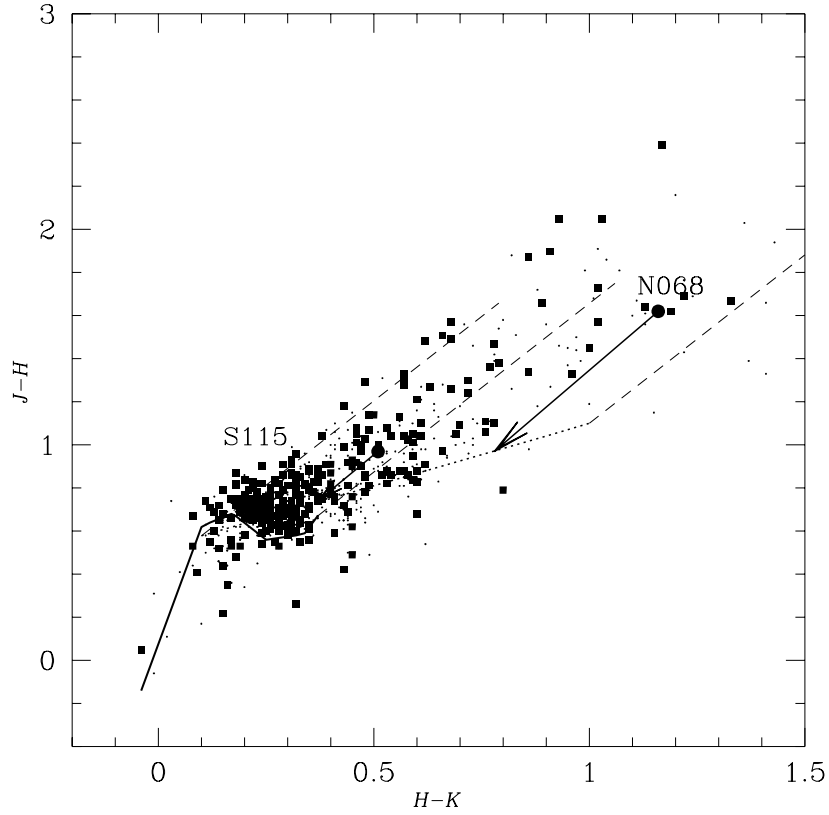


Fig. 9.— Observed infrared color-color diagram of sources located in the fields of the ACIS camera. The *filled squares* denote stars with X-ray counterparts, and the *dots* mark the position of stars without X-ray counterparts. The *thick line* marks the location of main sequence colors, the *dotted line* the locus of CTTs from Meyer et al. (1997), and the *dashed lines* are reddening vectors; the length corresponds to $A_V = 10$ magnitudes.

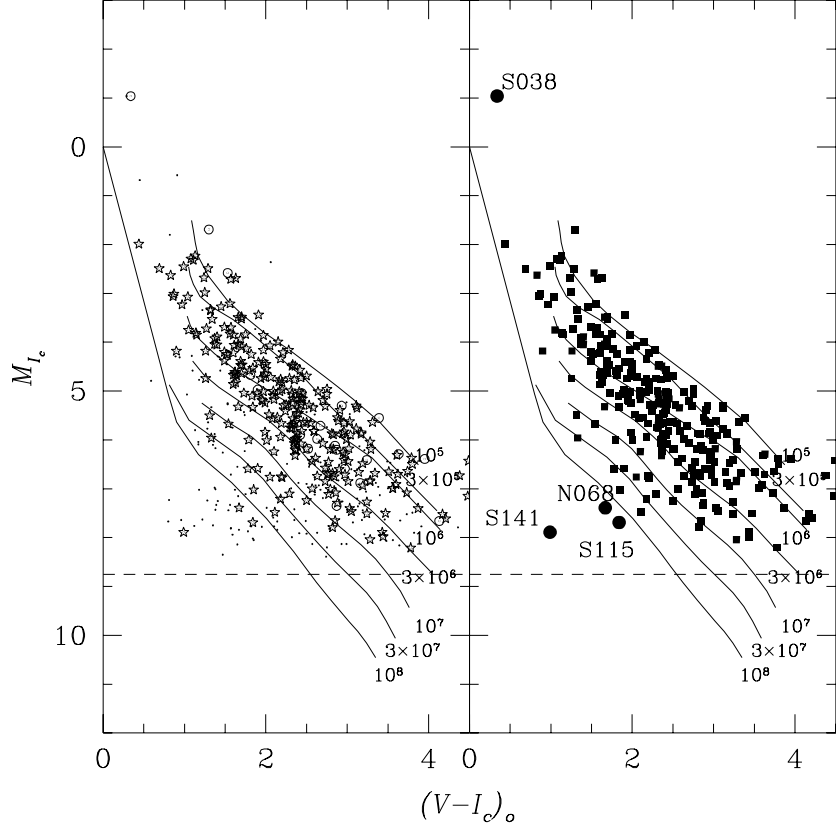


Fig. 10.— Dereddened optical color magnitude diagrams of sources located in the fields of the ACIS camera. In the left panel, *open circles* denote stars with X-ray counterparts and $L_x/L_{\text{bol}} < 10^{-4}$, *stars* denote sources with X-ray counterparts and $L_x/L_{\text{bol}} \geq 10^{-4}$, and the *dots* mark the position of stars without X-ray counterparts. In the right panel, only optical sources with X-ray counterparts are plotted. The dashed line corresponds to $M_{I_c} = 8.75$ mag., which is the lower limit for a low mass star rotating at the saturation level ($\log(L_x/L_{\text{bol}}) = -3$). The solid lines denote isochrones from D’Antona & Mazzitelli (1998).

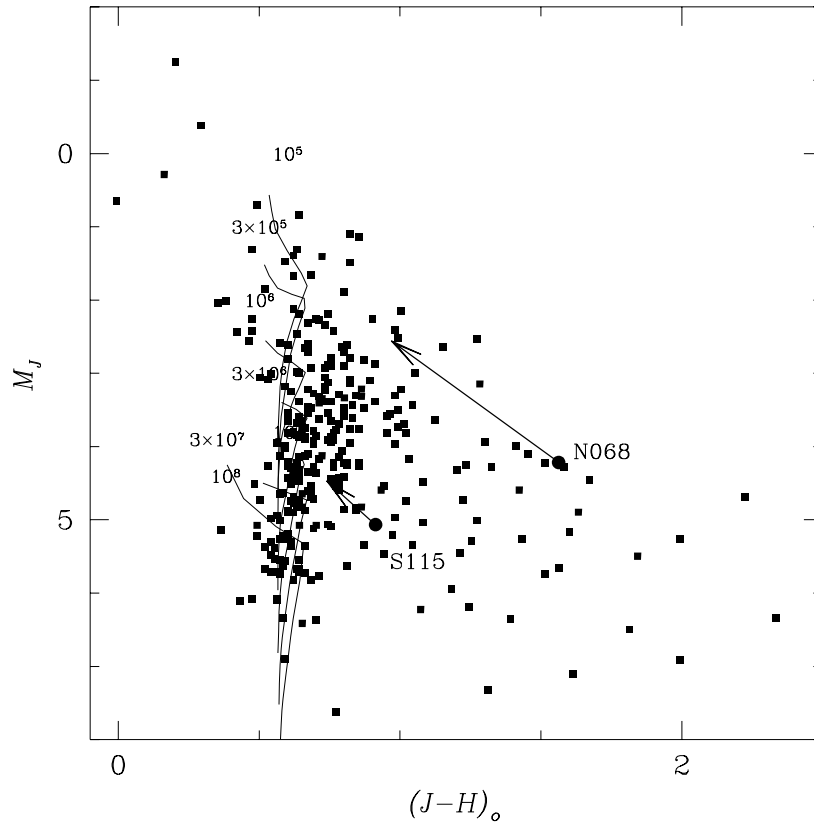


Fig. 11.— Dereddened infrared color magnitude diagram of sources located in the fields of the ACIS camera. Only infrared sources with X-ray counterparts are plotted. The solid lines denote isochrones from D’Antona & Mazzitelli (1998).

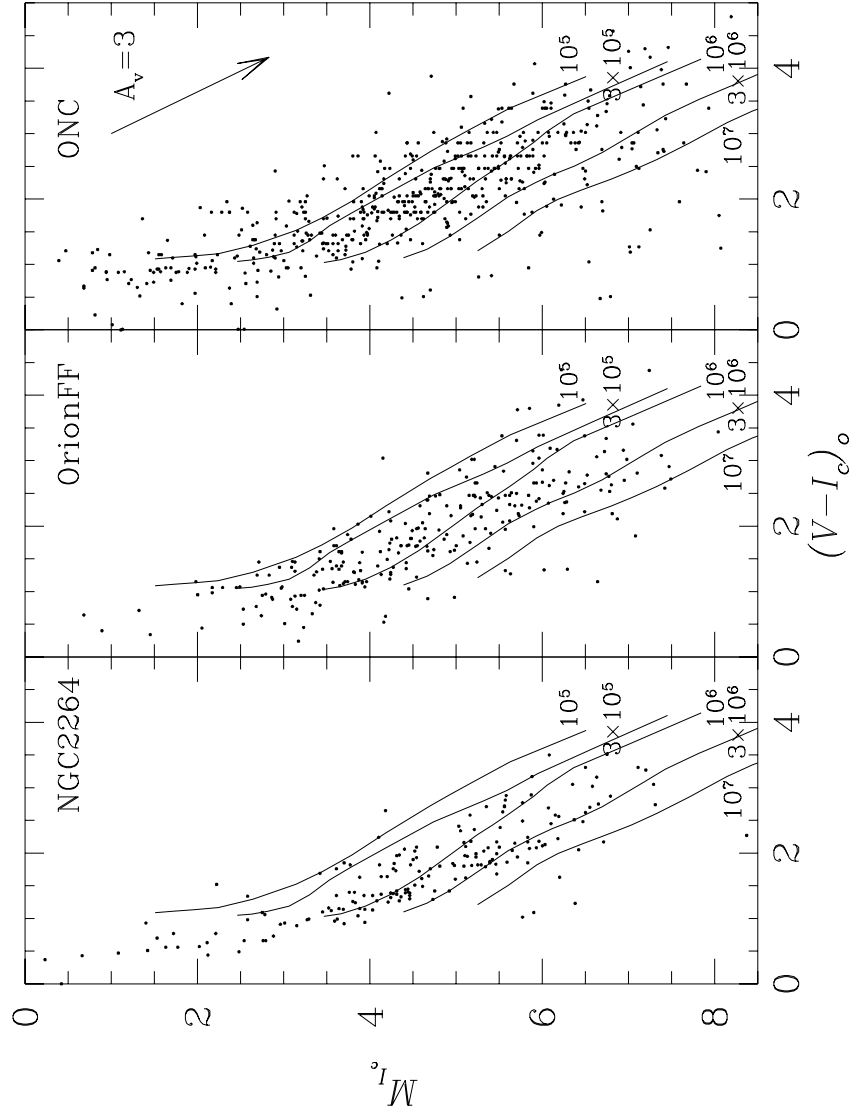


Fig. 12.— Dereddened optical color magnitude diagrams of X-ray selected samples in NGC 2264 (left panel), Orion Flanking Fields (central panel), and Orion Nebula Cluster (ONC, right panel). The solid lines denote isochrones from D’Antona & Mazzitelli (1998). The range in color selected for age comparison is $1.0 < (V - I_c)_o < 2.5$.

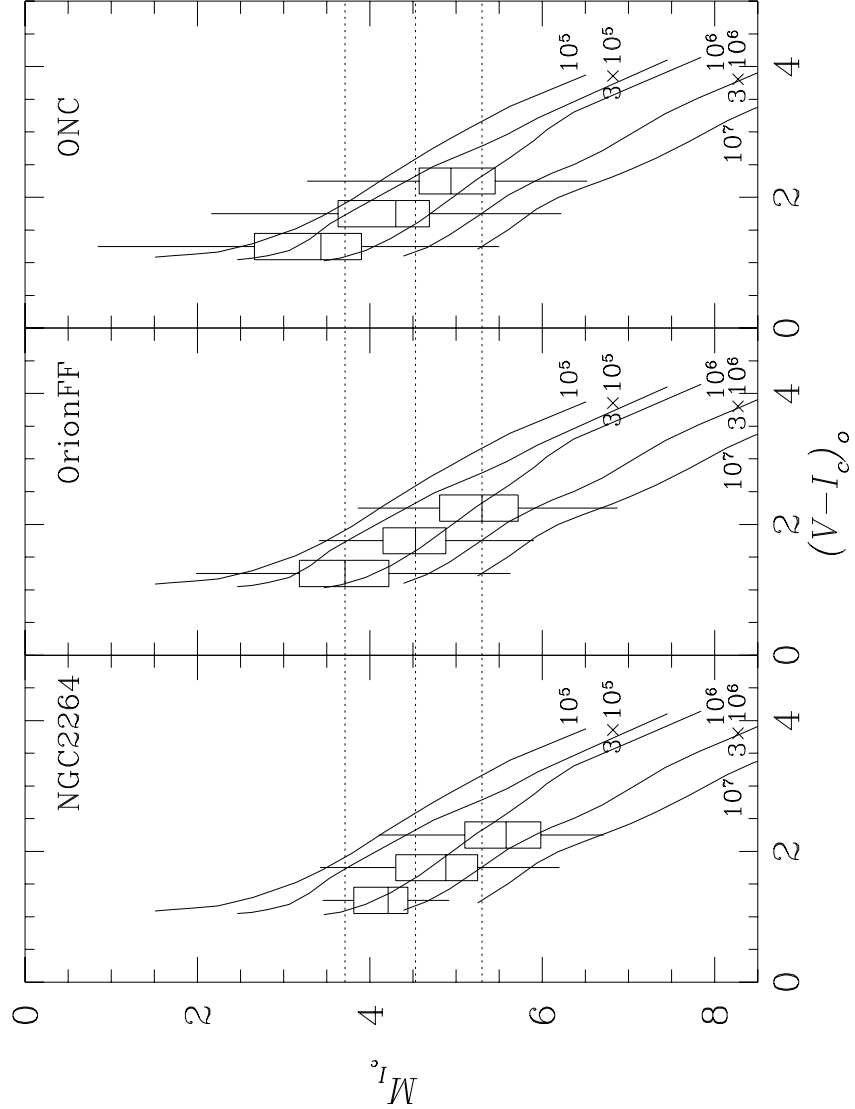


Fig. 13.— Dereddened optical color magnitude diagrams of X-ray selected samples in NGC 2264 (left panel), Orion Flanking Fields (central panel), and ONC (right panel), plotted as statistical boxes. Each box corresponds to a range in $(V - I_c)_o$ of 0.5 magnitudes. The central horizontal line of each box is the median M_{I_c} in the respective color range, the bottom and the top lines show its inter-quartile range and the vertical lines coming out of the box mark the position of the adjacent points of the sample. The horizontal dotted lines show the median M_{I_c} for the Orion Flanking Field sample. There is a consistent age difference among the three X-ray samples. The Orion Nebula Cluster sample is the youngest and the NGC 2264 sample is the oldest.

Table 1. The Catalog of X-ray Sources^a.

X-ID	Name	RA	DEC	ϕ	R_{ext}	f_{PSF}	t_{eff}	$C. R.$	Flux	$\log(L_x)$	$P_c(\chi^2)$	Comments ^b
(1)	(2)	(2000)	(2000)	($^\circ$)	($''$)	(7)	(ks)	(count/ks)	(erg/cm ² /s)	log(erg/s)	%	(13)
North Orion Flanking Field (NOFF)												
N001	CXORRS J053442.6-044215	5 34 42.70	-4 42 15.294	10.93	17.50	1.00	35.9	17.25	0.114E-12	30.48	93	
N002	CXORRS J053444.5-044214	5 34 44.53	-4 42 14.807	10.55	16.30	1.00	36.4	12.88	0.848E-13	30.35	0	v,s
N004	CXORRS J053448.2-044740	5 34 48.24	-4 47 40.865	7.77	9.50	0.98	40.9	36.05	0.237E-12	30.80	0	v,s
N005	CXORRS J053448.5-044956	5 34 48.60	-4 49 56.658	7.78	8.70	0.96	24.7	1.56	0.103E-13	29.43	99	
N007	CXORRS J053451.0-044341	5 34 51.05	-4 43 41.614	8.39	10.10	0.98	38.7	10.48	0.690E-13	30.26	0	v,f
N008	CXORRS J053451.2-044757	5 34 51.28	-4 47 57.405	7.00	9.40	0.99	41.6	55.40	0.365E-12	30.98	23	v
N010	CXORRS J053452.4-044941	5 34 52.46	-4 49 41.023	6.85	6.70	0.97	36.5	1.04	0.684E-14	29.26	100	
N011	CXORRS J053453.0-044811	5 34 53.02	-4 48 11.677	6.55	6.20	0.96	40.5	0.44	0.290E-14	28.88	100	
N012	CXORRS J053453.8-044340	5 34 53.82	-4 43 40.195	7.83	8.80	0.98	36.7	0.44	0.290E-14	28.88	100	
N015	CXORRS J053454.3-045413	5 34 54.31	-4 54 13.447	8.63	10.70	0.97	40.2	2.10	0.138E-13	29.56	97	
N016	CXORRS J053454.4-044540	5 34 54.44	-4 45 40.342	6.73	6.50	0.97	41.8	0.26	0.171E-14	28.66	100	
N017	CXORRS J053454.5-045604	5 34 54.58	-4 56 4.736	9.96	14.40	0.98	32.5	3.88	0.255E-13	29.83	99	
N018	CXORRS J053455.1-044827	5 34 55.12	-4 48 27.968	6.05	5.30	0.96	40.6	24.67	0.162E-12	30.63	2	v
N019	CXORRS J053455.6-045611	5 34 55.67	-4 56 11.579	9.89	14.20	0.98	39.3	3.78	0.249E-13	29.82	99	
N020	CXORRS J053456.3-044548	5 34 56.31	-4 45 48.316	6.25	5.70	0.97	37.7	1.14	0.750E-14	29.30	100	x
N021	CXORRS J053456.3-044437	5 34 56.39	-4 44 37.961	6.77	6.60	0.97	41.5	1.79	0.118E-13	29.49	100	x
N022	CXORRS J053456.8-044605	5 34 56.81	-4 46 5.044	6.01	5.30	0.97	39.8	8.12	0.534E-13	30.15	95	
N025	CXORRS J053457.9-044913	5 34 57.90	-4 49 13.139	5.43	4.40	0.95	19.6	14.61	0.961E-13	30.40	90	
N026	CXORRS J053458.2-045052	5 34 58.22	-4 50 52.031	5.86	5.00	0.96	40.1	0.27	0.178E-14	28.67	100	
N027	CXORRS J053459.3-045011	5 34 59.35	-4 50 11.837	5.36	4.30	0.95	42.7	2.40	0.158E-13	29.62	89	
N029	CXORRS J053459.6-044756	5 34 59.63	-4 47 56.143	4.92	3.70	0.95	43.4	0.68	0.447E-14	29.07	100	x
N030	CXORRS J053459.7-045158	5 34 59.70	-4 51 58.602	6.18	5.50	0.96	42.0	0.62	0.408E-14	29.03	98	
N031	CXORRS J053459.8-045526	5 34 59.87	-4 55 26.028	8.66	10.80	0.98	40.3	1.18	0.776E-14	29.31	100	
N034	CXORRS J053500.7-044649	5 35 0.80	-4 46 49.233	4.85	3.60	0.95	34.8	1.12	0.737E-14	29.29	99	
N035	CXORRS J053500.9-044819	5 35 0.92	-4 48 19.319	4.60	3.30	0.95	43.7	0.93	0.612E-14	29.21	98	
N037	CXORRS J053501.9-044115	5 35 1.96	-4 41 15.366	8.22	9.70	0.98	40.8	4.65	0.306E-13	29.91	13	v
N038	CXORRS J053502.0-044731	5 35 2.09	-4 47 31.843	4.36	3.00	0.95	34.9	1.14	0.750E-14	29.30	100	
N039	CXORRS J053502.3-044755	5 35 2.33	-4 47 55.508	4.21	2.90	0.95	32.3	2.64	0.174E-13	29.66	98	x

^aTable available electronically.

^bv: variable star; f: flare-like light curve; p: possible flare in the light curve; s: steady increase or decrease in the light curve; c: source confusion, see details in Sec.4.1;x: source detected only in X-rays, see details in Sec.4.2

Table 2. Spectral Properties of Bright Sources.

X-ID	Optical ID	<i>C. R.</i> (counts/ks)	kT1 (keV)	kT2 (keV)	Flux ^a (10 ⁻¹³ erg/cm ² /s)
North Orion Flanking Field (NOFF)					
N093	Par 1817	209.4	0.77	3.40	14.20
N256	Par 2257	65.6	0.70	2.87	4.03
N218	Par 2140	60.6	0.56	1.96	3.61
N087	Par 1798	56.0	1.05	3.62	3.78
N008	Par 1621	55.4	0.40	2.63	3.60
N097	Par 1834	52.5	0.00	3.58	3.35
N126	Par 1950	43.5	0.65	2.22	2.65
N044	Par 1701	35.4	0.00	2.74	2.54
N004	Par 1598	36.0	0.00	2.11	2.21
N137	Par 1967	30.3	0.31	1.39	1.88
N165	Par 2043	41.4	0.30	1.31	2.54
N124	Par 1935	27.8	0.00	1.23	1.65
N190	Par 2081	29.5	0.85	4.40	1.77
N222	Par 2145	27.0	0.61	2.40	1.54
N018	Par 1651	24.7	0.84	3.88	1.60
N195	R01 2133	21.1	0.40	3.25	1.25
N080	Par 1778	20.3	0.00	4.02	1.16
N208	Par 2109	17.0	0.24	1.07	0.91
N081	SMMV 1944	17.3	0.00	1.96	1.01
N156	Par 2017	67.2	0.00	1.38	4.06
N046	Par 1710	16.4	0.89	4.36	0.95
N130	Par 1948	16.1	0.87	5.02	0.91
N001	R01 1413	17.2	0.00	6.76	0.82
N175	Par 2064	12.9	0.00	1.01	0.75
South Orion Flanking Field (SOFF)					
S249	Par 2069	200.9	0.85	3.71	13.30
S168	Par 1828	100.8	1.00	4.80	7.21
S238	Par 2048	103.8	0.66	3.34	7.25
S020	Par 1553	52.0	0.70	2.43	3.40
S198	Par 1929	37.5	0.66	2.23	2.41
S040	Par 1756	34.7	0.77	2.70	2.16
S183	Par 1874	31.6	1.00	4.45	2.13
S152	Par 1787	27.3	1.33	5.82	1.85
S058	Par 1643	26.5	0.64	2.02	1.34
S172	Par 1846	21.2	0.64	2.65	1.26
S202	Par 1942	19.5	0.78	2.66	1.12
S174	Par 1848	19.5	0.86	3.70	1.14
S022	Par 1564	17.8	0.64	1.63	1.12
S047	Par 1613	16.0	0.69	1.76	0.86
S016	Par 1535	15.4	0.64	1.63	0.85
S039	Par 1616	15.6	0.64	1.47	0.85
S176	Par 1876	14.4	0.81	3.36	0.86
S079	R01 1603	13.1	0.32	3.58	0.64
S025	Par 1571	13.4	1.04	1.88	0.84
S104	CHS 7005	21.2	0.00	0.00	0.96

^aFlux determined from models of mean plasma temperatures

Table 3. Optical/Infrared Sources with X-ray counterparts^a.

Name	RA (2000)	DEC (2000)	X-ID	U mag	V mag	I _c mag	J mag	H mag	K mag
R01 1413	5 34 42.616	-4 42 14.86	N001	...	18.79	15.52	13.07	10.99	9.94
Par 1567	5 34 44.512	-4 42 13.71	N002	0.04	15.38	13.53	12.36	11.49	10.89
Par 1598	5 34 48.155	-4 47 39.98	N004	0.11	16.63	14.08	12.05	10.73	9.97
CHS 5807	5 34 48.548	-4 49 56.72	N005	13.97	12.07
Par 1620	5 34 50.988	-4 43 41.35	N007	...	16.02	13.60	12.14	11.09	10.43
Par 1621	5 34 51.204	-4 47 56.91	N008	...	15.85	13.45	11.88	10.66	9.96
R01 1536	5 34 52.410	-4 49 40.29	N010	19.34	16.40	13.76	12.45
Par 1639	5 34 52.963	-4 48 10.56	N011	17.10	15.20	...	12.23
R01 1563	5 34 53.670	-4 43 40.69	N012	18.12	15.82	14.57	13.95
2MASS J05345431-0454129	5 34 54.313	-4 54 13.447	N015	14.81	12.42
R01 1570	5 34 54.391	-4 45 39.22	N016	19.70	16.11	13.83	13.11
R01 1572	5 34 54.501	-4 56 4.96	N017	18.05	14.65	12.11	10.93
Par 1651	5 34 55.052	-4 48 27.54	N018	0.47	16.27	14.12	12.44	11.13	10.41
R01 1586	5 34 55.574	-4 56 11.23	N019	19.11	15.25	12.47	11.00
CHS 6568	5 34 56.817	-4 46 4.78	N022	11.46
R01 1610	5 34 57.827	-4 49 12.54	N025	16.99	14.43	12.73	11.91
R01 1620	5 34 58.184	-4 50 51.45	N026	18.61	15.72	13.30	12.38
Par 1672	5 34 59.269	-4 50 11.41	N027	15.85	13.38	11.77	10.93
R01 1635	5 34 59.636	-4 51 57.50	N030	21.60	16.58	13.94	12.94
2MASS J05345988-0455272	5 34 59.874	-4 55 26.028	N031	17.05	14.02
R01 1647	5 35 0.740	-4 46 49.07	N034	16.52	13.99	12.44	11.69
R01 1651	5 35 0.846	-4 48 18.71	N035	17.23	14.22	12.38	11.58
R01 1659	5 35 1.890	-4 41 14.54	N037	1.35	...	18.86	15.55	13.22	12.14
R01 1660	5 35 2.000	-4 47 30.73	N038	21.16	15.93	13.49	12.86
Par 1692	5 35 2.303	-4 49 15.92	N040	0.24	...	16.74	14.28	12.70	11.88
R01 1663	5 35 2.574	-4 49 29.12	N042	...	17.68	14.87	12.60	11.09	10.22
Par 1700	5 35 2.891	-4 48 32.54	N043	...	16.57	16.52	14.61	13.21	12.51
Par 1701	5 35 3.229	-4 49 20.29	N044	...	14.31	13.01	11.32	9.96	9.08
R01 1677	5 35 3.252	-4 56 42.63	N045	...	18.24	15.60	13.58	12.33	11.57
Par 1710	5 35 3.622	-4 50 52.77	N046	...	16.47	15.11	13.19	11.47	10.36
2MASS J05350376-0447516	5 35 3.748	-4 47 51.576	N047	14.24	13.47
Par 1709	5 35 4.292	-4 46 42.20	N048	9.79	9.26
2MASS J05350469-0452418	5 35 4.668	-4 52 41.560	N049	14.35	12.67

^aTable available electronically.

Table 4. Cross identification of sources with optical/infrared counterparts^a.

X-ID	Par name ^b	R01 name ^c	CHS name ^d	2MASS name ^e	Other names ^f
N001	...	R01 1413	CHS 5282	2MASS J05344268-0442148	SMMV 1089
N002	Par 1567	R01 1429	CHS 5438	2MASS J05344454-0442146	Tian 125,ROSAT 42,SMMV 1126
N004	Par 1598	R01 1483	...	2MASS J05344823-0447401	ROSAT 52
N005	CHS 5807	2MASS J05344854-0449568	...
N007	Par 1620	R01 1521	...	2MASS J05345106-0443414	...
N008	Par 1621	R01 1522	CHS 6064	2MASS J05345128-0447570	Einstein 56,ROSAT 59
N010	...	R01 1536	...	2MASS J05345249-0449404	...
N011	Par 1639	R01 1542	...	2MASS J05345302-0448104	...
N012	...	R01 1563	...	2MASS J05345374-0443407	...
N015	2MASS J05345431-0454129	...
N016	...	R01 1570	...	2MASS J05345446-0445393	...
N017	...	R01 1572	...	2MASS J05345458-0456053	...
N018	Par 1651	R01 1578	CHS 6412	2MASS J05345513-0448277	ROSAT 72
N019	...	R01 1586	CHS 6469	2MASS J05345566-0456117	...
N022	CHS 6568	2MASS J05345682-0446047	...
N025	...	R01 1610	...	2MASS J05345791-0449127	SMMV 1452
N026	...	R01 1620	...	2MASS J05345826-0450517	...
N027	Par 1672	R01 1633	...	2MASS J05345935-0450117	...
N030	...	R01 1635	...	2MASS J05345971-0451578	...
N031	2MASS J05345988-0455272	...
N034	...	R01 1647	...	2MASS J05350082-0446491	...
N035	...	R01 1651	...	2MASS J05350093-0448188	...
N037	...	R01 1659	CHS 7084	2MASS J05350196-0441145	...
N038	...	R01 1660	...	2MASS J05350208-0447308	...
N040	Par 1692	R01 1662	...	2MASS J05350238-0449161	...
N042	...	R01 1663	...	2MASS J05350265-0449293	...
N043	Par 1700	R01 1668	CHS 7175	2MASS J05350298-0448326	...
N044	Par 1701	R01 1676	CHS 7211	2MASS J05350326-0449209	Tian 158
N045	...	R01 1677	...	2MASS J05350333-0456430	...
N046	Par 1710	R01 1678	CHS 7251	2MASS J05350370-0450530	...
N047	2MASS J05350376-0447516	...
N048	Par 1709	2MASS J05350421-0446435	Tian 161
N049	2MASS J05350469-0452418	...
N050	2MASS J05350481-0447089	...

^aTable available electronically.

^bParenago (1954).

^cRebull (2001).

^dCarpenter et al. (2001).

^e2MASS Catalog.

^fSMMV (Stassun et al. (1999)); Tian (Tian et al. (1996)); ROSAT (Gagne & Caillault (1994)); Einstein (Gagne et al. (1995)); HBC (Herbig & Bell (1988)); JW (Jones & Walker (1988)); H97 (Hillenbrand (1997)); Feigelson (Feigelson et al. (2002)); HBJM (Herbst et al. (2001)).

Table 5. Upper limits for some optical/infrared stars in the Chandra field.

Par Name	R Name	CHS Name	2MASS Name	Other Names	Counts (counts)	<i>C. R.</i> (counts/ks)	Flux (10^{-13} erg/cm ² /s)	log(L _x) log(erg/s)
...	...	CHS 10870	< 6.30	< 0.3447	<0.0227	< 28.78
Par 2083	Tian 250	<10.70	< 0.4994	<0.0329	< 28.94
Par 2131	2MASS J05353948-0451216	Tian 258	< 9.80	< 0.2455	<0.0161	< 28.63
Par 1654	R01 1599	...	2MASS J05345622-0445574	Tian 150	< 8.00	< 0.2016	<0.0133	< 28.54
Par 1708	2MASS J05350478-0443546	Tian 162	< 8.40	< 0.2328	<0.0153	< 28.61
...	...	CHS 8034	2MASS J05351065-0442075	...	< 6.30	< 0.1464	<0.0096	< 28.41
...	...	CHS 8467	2MASS J05351406-0453112	...	< 5.10	< 0.1671	<0.0110	< 28.46
...	R01 1937	CHS 9321	2MASS J05351974-0448180	...	< 3.00	< 0.1881	<0.0124	< 28.51
...	R01 1720	...	2MASS J05350693-0449097	...	<13.90	< 0.8425	<0.0554	< 29.17
...	R01 1806	...	2MASS J05351282-0539077	JW 398	< 3.00	< 0.2237	<0.0150	< 28.60
...	...	CHS 9056	2MASS J05351795-0535157	JW 579,SMMV 2470	< 6.70	< 0.1530	<0.0103	< 28.43
...	2MASS J05351898-0537234	HBJM 10548	< 3.80	< 0.1427	<0.0096	< 28.40
...	JW 618	< 5.60	< 0.1889	<0.0127	< 28.53
Par 1810	R01 1795	...	2MASS J05351235-0536403	JW 384	<10.10	< 0.4175	<0.0280	< 28.87
Par 1898	2MASS J05351596-0539147	JW 514,Tian 196	< 3.00	< 0.1990	<0.0134	< 28.55
...	R01 1949	...	2MASS J05352074-0537536	JW 667	< 8.50	< 0.3344	<0.0225	< 28.77
...	R01 1451	...	2MASS J05344609-0537312	JW 79	<12.10	< 0.3498	<0.0235	< 28.79

Table 6. Median and Quartile Values for NGC 2264, Orion Flanking Fields, and Orion Nebula Cluster

Color Range	NGC 2264			Orion Flanking Fields			Orion Nebula Cluster		
	Upper Quartile	Median	Lower Quartile	Upper Quartile	Median	Lower Quartile	Upper Quartile	Median	Lower Quartile
1.0–1.5	3.81	4.21	4.44	3.18	3.71	4.22	2.66	3.43	3.90
1.5–2.0	4.30	4.88	5.25	4.15	4.53	4.88	3.63	4.30	4.69
2.0–2.5	5.10	5.58	5.98	4.81	5.30	5.72	4.57	4.94	5.45